

# A General Model for Preferential Hetero-oligomerization of LIN-2/7 Domains

## MECHANISM UNDERLYING DIRECTED ASSEMBLY OF SUPRAMOLECULAR SIGNALING COMPLEXES\*

Received for publication, June 15, 2005, and in revised form, August 12, 2005. Published, JBC Papers in Press, September 7, 2005, DOI 10.1074/jbc.M506536200

Keiko Y. Petrosky<sup>‡</sup>, Horng D. Ou<sup>‡</sup>, Frank Löhr<sup>§</sup>, Volker Dötsch<sup>§</sup>, and Wendell A. Lim<sup>¶1</sup>

From the <sup>‡</sup>Biophysics Graduate Program and the <sup>¶</sup>Department of Cellular and Molecular Pharmacology, University of California, San Francisco, California 94143 and the <sup>§</sup>Institute for Biophysical Chemistry, University of Frankfurt, Frankfurt am Main, 60439 Germany

LIN-2/7 (L27) domains are protein interaction modules that preferentially hetero-oligomerize, a property critical for their function in directing specific assembly of supramolecular signaling complexes at synapses and other polarized cell-cell junctions. We have solved the solution structure of the heterodimer composed of the L27 domains from LIN-2 and LIN-7. Comparison of this structure with other L27 domain structures has allowed us to formulate a general model for why most L27 domains form an obligate heterodimer complex. L27 domains can be divided in two types (A and B), with each heterodimer comprising an A/B pair. We have identified two keystone positions that play a central role in discrimination. The residues at these positions are energetically acceptable in the context of an A/B heterodimer, but would lead to packing defects or electrostatic repulsion in the context of A/A and B/B homodimers. As predicted by the model, mutations of keystone residues stabilize normally strongly disfavored homodimers. Thus, L27 domains are specifically optimized to avoid homodimeric interactions.

Accurate transmission of cell signaling information often requires the proper co-assembly of partner proteins (1). In eukaryotes, many of these assembly interactions are mediated by modular protein-protein interaction domains. Because these modular domains often compose large families of domains, discrimination between related domains is critical; lack of specificity leads to promiscuous interactions and improper signaling (2). Thus, it is important to understand the molecular basis by which protein interaction domains recognize their correct partner but simultaneously discriminate against closely related but incorrect partners.

Modular interaction domains play a central role in organizing polarized sites of cell-cell communication. At such sites of polarization, signaling proteins are organized into specific assemblies by scaffold proteins. The postsynaptic density in neurons (3, 4), tight junction in epithelial cells (5), and immune synapse (6) are examples of highly organized signaling assembly coordinated by such scaffold proteins. In neurons and epithelial cells, PDZ (PSD95/DLG-1/ZO-1) domain-contain-

ing scaffold molecules play a central role in directing the trafficking and assembly of receptors and downstream effectors (7).

More recently, many of these PDZ domain-containing scaffold proteins have been found to interact with one another to form higher order supramolecular complexes (8, 9). These higher order interactions are mediated primarily by a novel type of protein interaction domain referred to as the LIN-2/7 (L27)<sup>2</sup> domain (10–14) (Fig. 1A). L27 domains have been found only within metazoan scaffold proteins (15), and several examples are shown in Fig. 1B. To date, there are 34 known human proteins containing L27 domains (15). Several of these scaffold proteins form specific heterotrimeric complexes (16–19), the assembly of which is mediated directly by L27 domains. For example, in *Caenorhabditis elegans*, the epidermal growth factor receptor LET-23 is targeted to the basolateral surface by a complex of the proteins LIN-2, LIN-7, and LIN-10 (16). Similar complexes are found in mammalian cells (17–19). L27 domain-containing complexes are organized at neural muscular junctions (20, 21), epithelial cell contacts (22–25), and immune synapses (26, 27). Thus, L27 domains appear to play a central role in the higher order organization of multi-scaffold assemblies.

Biochemical studies have revealed that known L27 domains are obligate hetero-oligomerization units (11). L27 domains, which are ~60 residues (28), are largely unfolded in isolation, but fold to form a helical heterodimer upon interaction with the proper heterotypic partner (11). In some cases, two heterodimers can further oligomerize to form a higher order tetramer (29–31). However, in all cases, all assemblies are built from the fundamental unit of a heterodimer. This core dimer unit displays an exclusive preference for heterodimerization *versus* homodimerization: typically, when only one L27 domain molecule is present, there is no evidence for folding into a homomer structure (11). The obligate heteromeric assembly of L27 domains is thought to be fundamental to its basic function of directing the formation of specific heteromeric supramolecular assemblies.

The structures of several L27 domain-containing complexes have been reported (29, 30), and mutational analysis has indicated that hydrophobic residues are involved in shape-complementary interactions across the dimer interface (30). However, little is understood about how L27 domains bind tightly to their correct heterotypic partners while showing almost no self-association. Here, we report the solution structure of the heterodimer composed of the LIN-7 L27 domain and the C-terminal L27 domain from LIN-2 (referred to as LIN-2C). By comparing this and other L27 domain heterodimer structures, we have formulated a general model for why most L27 domains form obligate

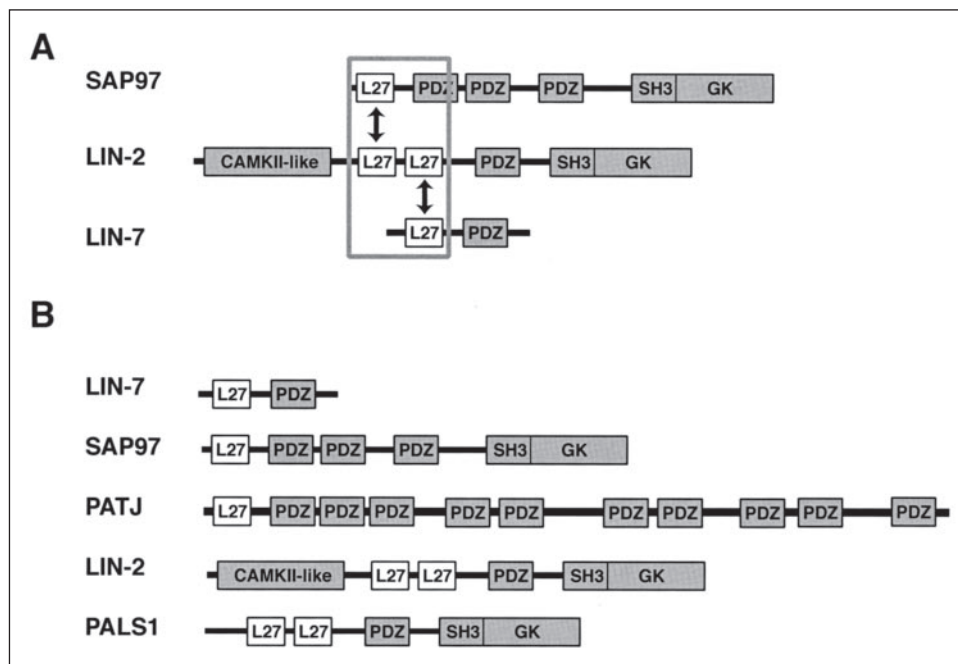
\* The costs of publication of this article were defrayed in part by the payment of page charges. This article must therefore be hereby marked "advertisement" in accordance with 18 U.S.C. Section 1734 solely to indicate this fact.

The atomic coordinates and structure factors (code 1ZL8) have been deposited in the Protein Data Bank, Research Collaboratory for Structural Bioinformatics, Rutgers University, New Brunswick, NJ (<http://www.rcsb.org/>).

<sup>1</sup> To whom correspondence should be addressed: Dept. of Cellular and Molecular Pharmacology, University of California, 600 16th St., San Francisco, CA 94143. Tel.: 415-502-8080; Fax: 415-514-4242; E-mail: wlim@itsa.ucsf.edu.

<sup>2</sup> The abbreviations used are: L27, LIN-2/7; GdnHCl, guanidine hydrochloride; HSQC, heteronuclear single quantum correlation; TROSY, transverse relaxation optimized spectroscopy; TOCSY, total correlation spectroscopy.

**FIGURE 1. Domain architecture and interactions of L27 domain-containing scaffold proteins.** *A*, a set of four L27 domains (boxed) mediate formation of a conserved heterotrimeric assembly of PDZ domain-containing membrane-associated guanylate kinase scaffold proteins that organize signaling complexes at cell-cell junctions. *Arrows* indicate specific interactions between L27 domains. The PDZ domains participate in interactions with receptors, signaling molecules, and cytoskeletal proteins. *B*, examples of L27 domain-containing proteins. *SH3*, Src homology-3 domain; *GK*, guanylate kinase domain; *CAMKII-like*, calcium/calmodulin-dependent protein kinase II-like domain.



heterodimers. L27 domains can be divided in two types, referred to as A and B (29), with each heterodimer comprising an A/B pair. We have identified two keystone positions that play a central role in discrimination between heterodimer and homodimer formation. The residues at these positions are energetically acceptable in the context of an A/B heterodimer, but would be destabilizing in the context of a hypothetical A/A or B/B homodimer, leading to packing defects or electrostatic repulsion. As predicted by the model, mutation of these keystone positions increases the stability of the normally strongly disfavored homodimers. Thus, L27 domains are specifically optimized by negative design: they are simultaneously optimized to maximize heterotypic complementarity and to avoid homotypic interactions.

## MATERIALS AND METHODS

**Cloning and Expression of Linked L27 Domains**—DNA regions encoding L27 domains were amplified by PCR (11). The regions cloned comprised *C. elegans* LIN-7A amino acids 115–180 (referred to as LIN-7) and *H. sapiens* LIN-2 amino acids 394–460 (referred to as LIN-2C). The mixed species LIN-7/LIN-2C pair (*C. elegans/Homo sapiens*) was previously shown to be particularly stable (11) and best suited for structural analysis.

L27 domains from LIN-7 and LIN-2C were expressed as a linked construct to ensure a 1:1 ratio and to improve solubility, a technique previously used to express the SAP97/LIN-2N L27 domain pair (29). PCR primers were used to engineer a Gly-Ser linker between the two L27 domains. The coding fragments were ligated into the expression vector pBH4, which provided an N-terminal His<sub>6</sub> tag for purification. All constructs were verified by sequencing on both strands. The LIN-7 L27 domain construct has been described previously (11). Keystone residues were mutated by QuikChange site-directed mutagenesis.

Protein constructs were expressed in *Escherichia coli* strain BL21 pLysS (Invitrogen). Cultures were grown in standard Luria broth at 32 °C and induced with 1 mM isopropyl 1-thio- $\beta$ -D-galactopyranoside at  $A_{600\text{ nm}} \sim 0.8$ . To obtain labeled protein constructs (<sup>15</sup>N, <sup>13</sup>C, and <sup>13</sup>C,<sup>15</sup>N; 70% deuterated) for NMR analysis, cultures were transferred to M9 minimal medium containing labeled <sup>15</sup>NH<sub>4</sub>Cl and/or [<sup>13</sup>C<sub>6</sub>]glucose before induction. Unlabeled protein constructs were harvested by cen-

trifugation after 3 h of growth, whereas labeled protein constructs were harvested after 5 h. Cell pellets were resuspended in ~25 ml of lysis buffer (50 mM Tris-Cl (pH 7.5) and 400 mM NaCl) per original liter of culture and subjected to freeze-thaw treatment. Cell suspensions were lysed by sonication and cleared by centrifugation at 15,000  $\times$  g. Wild-type and mutant constructs were expressed at similar levels.

The His<sub>6</sub> tag-containing proteins were purified under native conditions by nickel-nitrilotriacetic acid affinity chromatography (Qiagen Inc.). For NMR analysis, purified protein was dialyzed in 20 mM HEPES (pH 8.0) and 0.5 mM tris(2-carboxyethyl)phosphine hydrochloride for constructs containing cysteines, concentrated, and stored at –80 °C until used. For CD experiments, protein was stored in 50 mM phosphate buffer (pH 7.5), 10 mM NaCl, and 1 mM tris(2-carboxyethyl)phosphine hydrochloride for constructs containing cysteines.

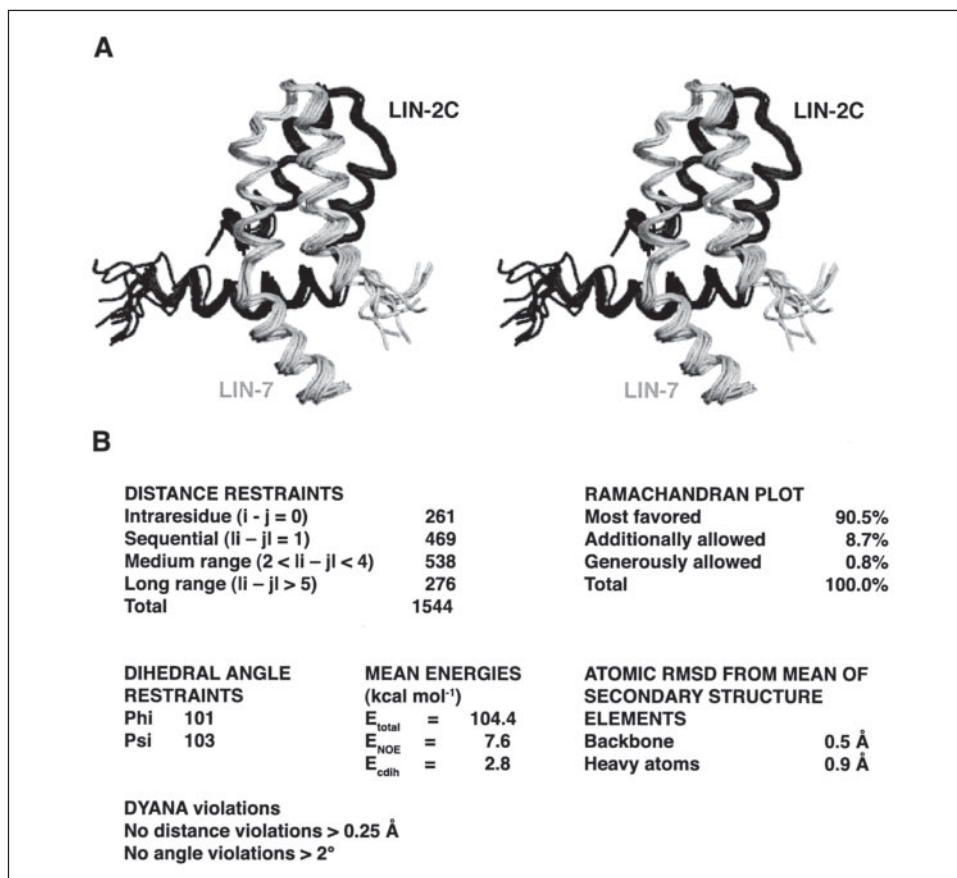
**NMR Structure Determination and Analysis**—NMR experiments were carried out at 25 °C on Bruker DRX500, DMX600, and Avance 700 spectrometers equipped with conventional <sup>1</sup>H{<sup>13</sup>C/<sup>15</sup>N} triple resonance probes and on Bruker DRX600, Avance800, and Avance900 spectrometers equipped with cryogenic <sup>1</sup>H{<sup>13</sup>C/<sup>15</sup>N} probes. Samples contained 2 mM protein in 90% H<sub>2</sub>O and 10% D<sub>2</sub>O with 20 mM HEPES (pH 8.0), 5 mM tris(2-carboxyethyl)phosphine hydrochloride, 0.05% 2,2-dimethylsilapentane-5-sulfonic acid, and 0.05% sodium azide.

Signal dispersion of the constructs was verified with <sup>15</sup>N heteronuclear single quantum correlation spectroscopy (HSQC) spectra. Sequential backbone assignments were derived from transverse relaxation optimized spectroscopy (TROSY)-type three-dimensional heteronuclear correlation experiments, including HNCO, HN(CA)CO, HN(CO)CACB, and HNCACB (32). Side chains were assigned through a combination of total correlation spectroscopy (TOCSY)-[<sup>15</sup>N,<sup>1</sup>H]-TROSY, (H)CC(CO)NH and HCC(CO)NH spectra (32). Distance constraints were derived from nuclear Overhauser effect correlation spectroscopy (NOESY)-[<sup>15</sup>N,<sup>1</sup>H]-TROSY, two types of NOESY-[<sup>13</sup>C,<sup>1</sup>H]-HSQC experiments optimized for CH<sub>3</sub> groups and aliphatic CH/CH<sub>2</sub> groups and a constant time NOESY-[<sup>13</sup>C,<sup>1</sup>H]-TROSY with mixing times ranging 70 to 120 ms (32).

Spectra were processed using XWIN-NMR (Bruker BioSpin Corp.) and analyzed using XEASY (34). Chemical shifts were referenced to

## A Model for Preferential L27 Domain Hetero-oligomerization

**FIGURE 2. NMR structure of the LIN-7/LIN-2C L27 domain dimer.** *A*, wall-eye stereo diagram showing 10 superimposed NMR-derived structures; *B*, structural statistics. *RMSD*, root mean square deviation.



2,2-dimethylsilapentane-5-sulfonic acid. Backbone dihedral angle restraints were derived from N, HN, C- $\alpha$ , and C- $\beta$  chemical shifts with the program TALOS (35). Structures were iteratively refined using the simulated annealing protocol of the torsion angle dynamics program DYANA (36). Nuclear Overhauser effect peak intensities were converted into upper distance bounds with the CALIBA function of DYANA. Of the final 100 structures calculated, the 10 conformers with the lowest target function values were selected for analysis. These structures were averaged, and the resulting structure was minimized in CNS (37) using conjugate gradient minimization. The resulting 10 best structures were assessed for overall quality using PROCHECK (see Fig. 2) (38). The coordinates have been deposited in the Protein Data Bank (code 1ZL8). The residues in the Protein Data Bank file (Leu<sup>5</sup>-Tyr<sup>53</sup> from the L27 domain of LIN-7 and Ser<sup>6</sup>-Ala<sup>59</sup> from the C-terminal domain of LIN-2) correspond to the numbering in Fig. 3. Note that residues not observed by NMR are not included in the Protein Data Bank file. Figures were generated using MolMol (39) and PyMOL (40). Contact maps were generated using CNS.

**Circular Dichroism**—CD spectroscopy was performed on a Jasco 715 spectropolarimeter. All scans were performed in a 1-cm quartz cuvette in 50 mM sodium phosphate buffer (pH 7.5), 10 mM NaCl, and 1 mM tris(2-carboxyethyl)phosphine hydrochloride for constructs containing cysteines. The CD spectra shown are the averages of two experiments. Data for wavelength scans were collected at 1-nm intervals with 1-s averaging time/data point and a total of 10 repetitions/scan. Data for guanidine hydrochloride (GdnHCl) denaturation studies were collected at 222 nm with 0.1 M denaturant intervals and with 60-s averaging time/data point and 60-s equilibration time/data point. Identical results were obtained with the wild-type protein for longer equilibration times (data not shown). Both orientations of linked domains were found to

behave identically in denaturant melts (data not shown). The midpoint of the unfolding transition is concentration-independent above 4  $\mu$ M for the wild-type construct (data not shown). For all experiments, the total L27 domain concentration was 10  $\mu$ M (10  $\mu$ M monomers and 5  $\mu$ M linked heterodimer).

## RESULTS

**Structure of the LIN-7/LIN-2C L27 Domain Heterodimer**—The structure of the LIN-7/LIN-2C heterodimer was solved by NMR as shown in Fig. 2. The two domains are expressed in a single covalently linked protein that yields improved expression and provides a 1:1 stoichiometry while not perturbing the structure of the complex (31). The unlinked LIN-7·LIN-2C complex was previously shown to exist primarily as a dimer (11). When covalently linked, the apparent molecular mass of the complex doubles (data not shown), consistent with formation of a tetramer at NMR and CD concentrations. A similar tetramer structure has recently been reported for a LIN-7·LIN-2C complex from mouse (31). The tetramer interface is discussed elsewhere in great detail (29, 31); here, we focused primarily on the interaction specificity within the core heterodimer unit.

The structure of the core heterodimer is similar to those of the previously solved L27 domain heterodimers, those involving SAP97/LIN-2N (29) and PATJ/PALS1N (30). (LIN-2 and PALS1 scaffold proteins each contain two L27 domains; the "N" indicates that these structures contain the N-terminal L27 domain.) Each individual monomer contains three  $\alpha$ -helices, with the first two helices from each monomer packing together to form a four-helix bundle that forms the core of the dimer. The third helices from the two monomers pack against one another and the bottom of the helical bundle, capping the hydrophobic core presented by the bundle. The overall heterodimer structure buries

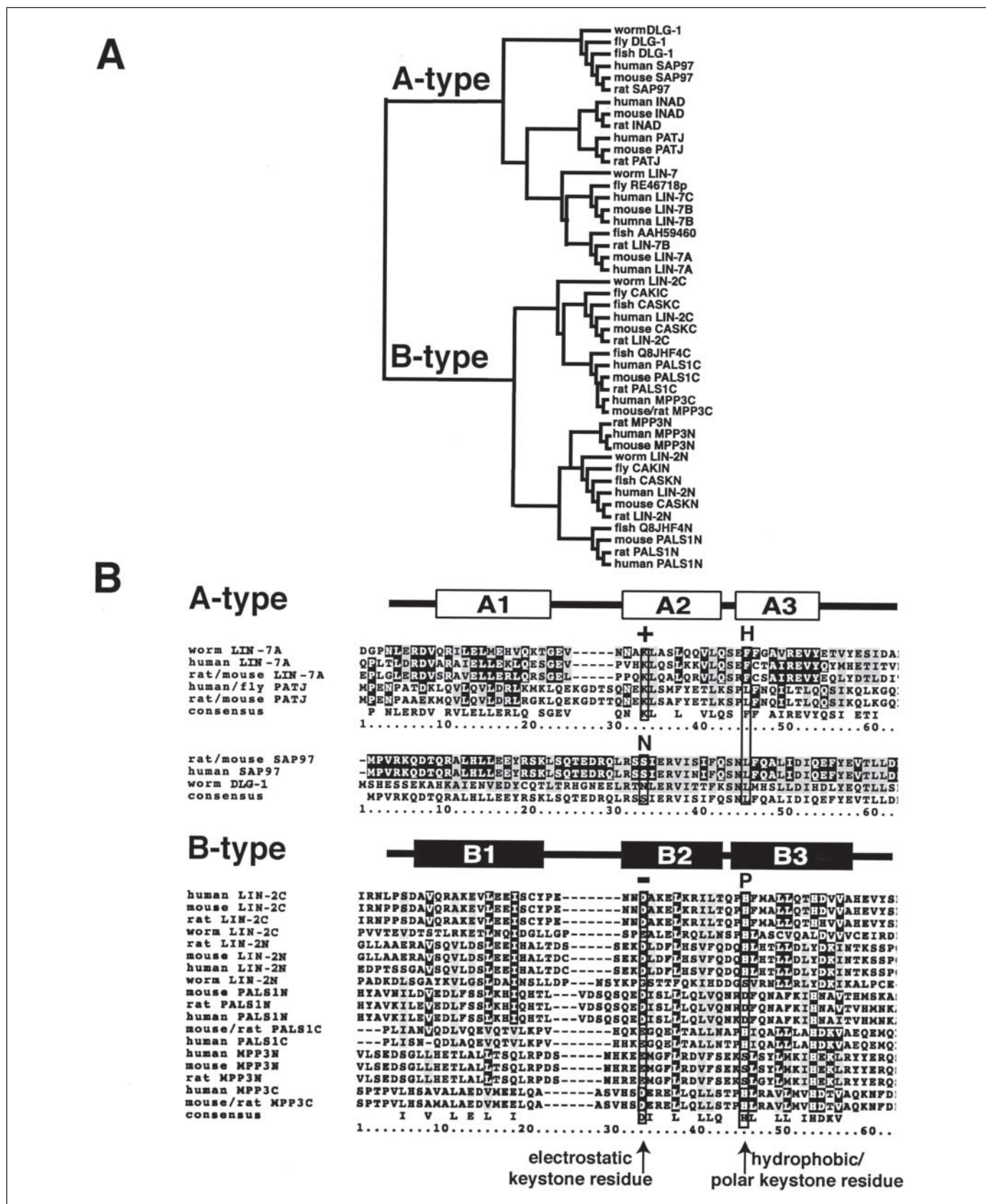
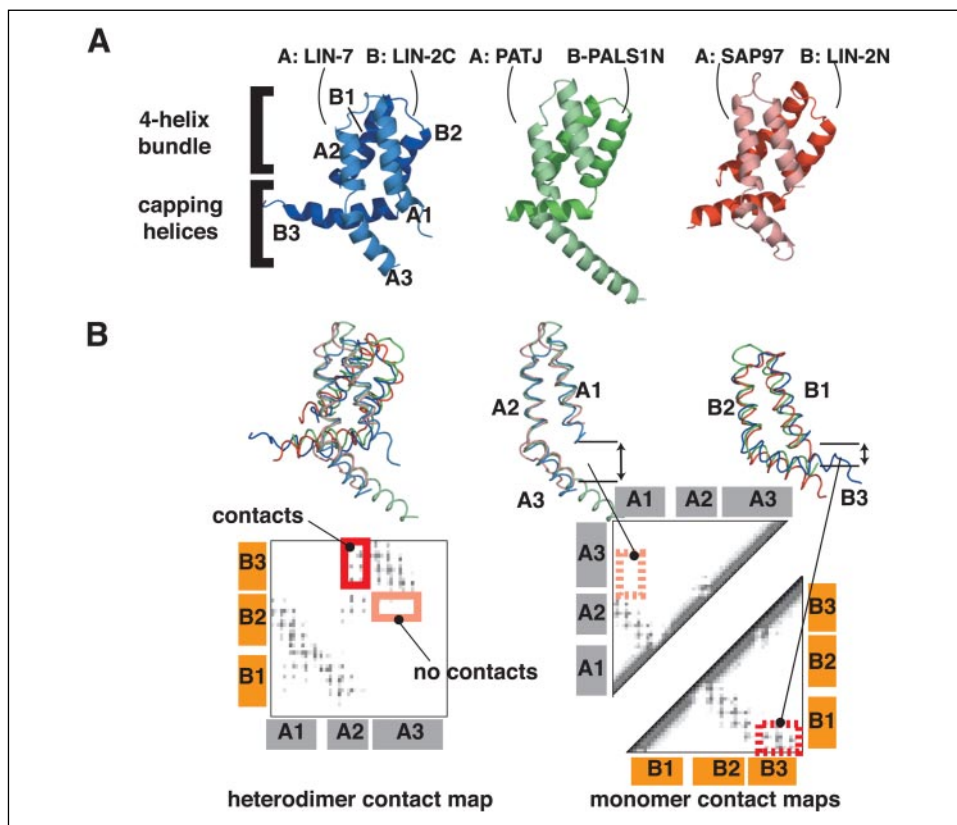


FIGURE 3. Sequence divergence between A- and B-type L27 domains. *A*, L27 domain sequences cluster into A- and B-type domains by sequence homology; *B*, sequence alignment of A- and B-type domains. We have identified two differentiating "keystone" positions. At the "electrostatic" keystone position, A-type domains generally have a positively charged residue (+), whereas B-type domains have a negatively charged residue (-). A subclass of A-type domains (SAP97 family members) have a neutral residue (N), the implications of which are reviewed under "Discussion." At the "hydrophobic/polar" keystone position, A-type domains have a conserved hydrophobic residue (H), which is polar in the B-type domains (P).

## A Model for Preferential L27 Domain Hetero-oligomerization

**FIGURE 4. Conserved structural asymmetry in the L27 domain A/B heterodimer.** *A*, structures of L27 domain heterodimers. The reported PATJ/PALS1N (Protein Data Bank code 1VF6) and SAP97/LIN-2N (code 1RSO) structures are tetrameric (dimer of a heterodimer). Only one heterodimer is shown: chains A and C are shown for the PATJ/PALS1N heterodimer, and chains A and B are shown for the SAP97/LIN-2N heterodimer. *B*, alignments of L27 domain heterodimers and individual monomers. Contact maps are shown of the PATJ/PALS1N heterodimer and individual monomers. Similar maps were observed for the other L27 domains. A 6-Å cutoff was used for contacts between C- $\alpha$ . Helices A3 and B3 adopt distinct conformations with respect to the central four-helix bundle: helix B3 makes more extensive contacts with helices A2 and B1.



a surface area of 2159 Å<sup>2</sup>, 69% of which is due to the packing interface of the central four-helix bundle.

**L27 Domains Fall into Two Distinct Sequence Types**—When aligned, all known L27 domain sequences segregate into two distinct types, referred to as A and B (29). The clustering of these two types is shown in a dendrogram and by sequence alignment in Fig. 3 (*A* and *B*). Strikingly, each pair of known interacting L27 domains involves the interaction of an A-type monomer with a B-type monomer (10–14). Not only are most monomers unable to self-associate, but they are also unable to interact with distinct monomers from within the same type (11, 12, 14). In the case of the LIN-7/LIN-2C heterodimer studied here, LIN-7 is the A-type monomer, whereas LIN-2C is a B-type monomer.

**Conserved Structural Asymmetry in L27 Domain Dimers**—A comparison of the three known L27 domain dimer structures is shown in Fig. 4*A*. These structures align well (LIN-7/LIN-2C *versus* PATJ/PALS1N root mean square deviation (C- $\alpha$ ) = 2.17 Å and LIN-7/LIN-2C *versus* SAP97/LIN-2N root mean square deviation (C- $\alpha$ ) = 3.45 Å) only when the same monomer subtypes are aligned (Fig. 4*B*). The other chains in the tetramer structures are similarly aligned. Careful examination revealed that there are distinct asymmetries between the A- and B-type monomer structures that are conserved across all known structures (31). Several key asymmetric features are highlighted in the contact maps shown in Fig. 4*B*. For the individual monomer units, in the B-type monomer, helix B1 and B3 come into close contact, whereas in the A-type monomer, helix A1 and A3 do not. In the dimer structure, helix B3 comes within 6 Å of helix A2, whereas helix A3 does not come closer than 10 Å to helix B2. These asymmetries can be understood by examining the overall dimer structure (Fig. 4*A*). Although helices A3 and B3 function together to cap the bottom end of the central four-helix bundle, helix B3 packs directly against the base of the bundle. In contrast, helix A3 primarily packs against helix B3.

**Keystone Positions: Potential Determinants of A- and B-type Monomer Structural Identity**—The well conserved structural asymmetry between A- and B-type monomers in three different L27 domain dimer structures suggests that there is a fundamental difference in monomer sequence that results in these clear structural differences. Thus, we carefully examined the sequences of A and B subtypes for potential keystone positions that are distinct in each type. Two strong candidate positions emerged. First, the third residue in helix 2 has distinct electrostatic properties; in A-type monomers, this residue is either positively charged or neutral, whereas in B-type monomers, it is almost always negatively charged. Additionally, the second residue in helix 3 has distinct hydrophobic *versus* polar character; in A-type monomers, this position is always a large hydrophobic residue, whereas in B-type monomers, it is a polar residue. These potential keystone positions are highlighted in the alignment shown in Fig. 3*B*. In the following two sections, we examine how these two keystone positions might contribute to preferential heterodimerization.

**The Hydrophobic/Polar Keystone Position**—The second residue in helix 3 is generally a large hydrophobic residue (Phe, Leu, or Met) in A-type L27 domains, whereas it is almost always a polar residue (His, Asp, or Ser) in B-type L27 domains (Fig. 3). Examination of L27 domain dimer structures revealed that this position is at the center of the conserved structural asymmetry. Helix A3 adopts a different orientation compared with helix B3 with respect to the main four-helix bundle. Because of this different orientation, as shown in Fig. 5*A*, the second residue in helix A3 (e.g. Phe<sup>41</sup> in LIN-7) points into the core of the protein, whereas the second residue in helix B3 (e.g. His<sup>39</sup> in LIN-2C) points toward the solvent. Thus, a possible model is that, to satisfy packing and hydrophobicity requirements, this position must be a hydrophobic residue in the A-type monomer, whereas the identity in the B-type monomer is not critical.

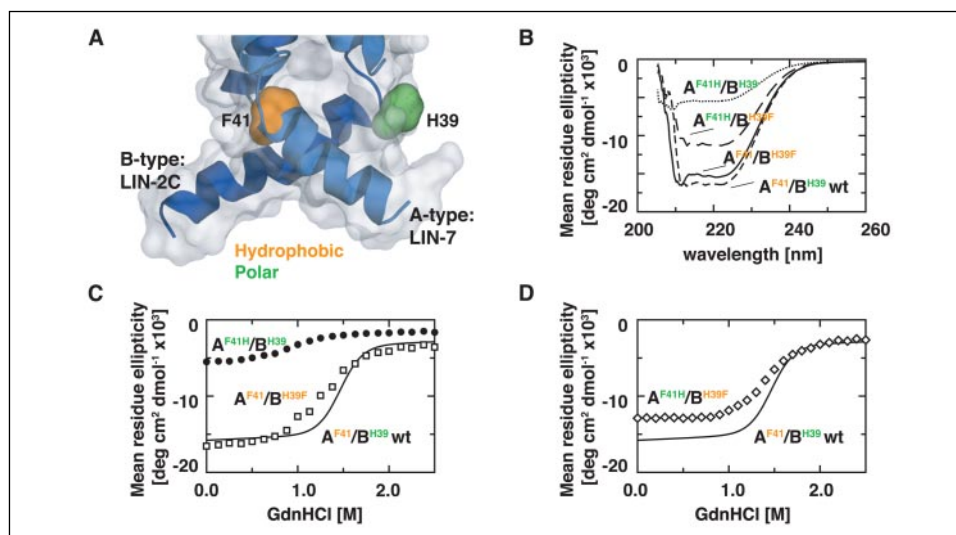


FIGURE 5. **Mutational analysis of the hydrophobic/polar keystone position.** *A*, the keystone residues at the beginning of helix 3 lie in different environments in the A- and B-type monomers (LIN-7/LIN-2C structure shown). The polar residue His<sup>39</sup> in the B-type monomer points away from the protein core, whereas the hydrophobic residue Phe<sup>41</sup> in the A-type monomer points into the central hydrophobic core formed by the four-helix bundle. *B*, the CD spectrum of the wild-type (wt) linked LIN-7/LIN-2C heterodimer indicates high helical content (—). Mutation of the polar residue to a hydrophobic residue (LIN-2C H39F; - - -) had little effect on structure, whereas mutation of the hydrophobic residue to a polar residue (LIN-7 F41H; ···) resulted in a significant loss of helical signal. Swapping hydrophobic and polar positions partially restored helical signal (LIN-7 F41H and LIN-2C H39F; - · -). *C*, GdnHCl (*GdnHCl*) denaturation curves show that the polar-to-hydrophobic mutant (H39F; □) was only mildly destabilized, whereas the hydrophobic-to-polar mutant (F41H; ●) failed to show a cooperative unfolding transition. *D*, swapping hydrophobic and polar positions restored significant stability (LIN-7 F41H and LIN-2C H39F; ◇). *deg*, degrees.

To test this model, we mutated these two positions in the context of a linked LIN-7/LIN-2C construct (A/B) (Fig. 5, *B–D*). The wild-type construct showed a highly helical CD spectrum and a cooperative GdnHCl denaturation transition, indicative of a well folded protein. However, when Phe<sup>41</sup> in the A-type monomer was mutated to histidine, the protein was destabilized, and helical structure was lost. In contrast, when His<sup>39</sup> in the B-type monomer was mutated to phenylalanine, there was minimal loss in stability. In addition, the mutation of this keystone residue in the PALS1 C-terminal L27 domain (B type) to another polar residue is functionally neutral (10). Thus, the keystone position must be hydrophobic in the A-type monomer (buried), whereas either a hydrophobic or polar residue can be tolerated in the B-type monomer (surface). Interestingly, although the F41H (A-type monomer) mutation is unstable, combining this with an additional mutation of H39F (B-type monomer) led to a stable construct. This finding suggests that there is not an absolute requirement that this position in the A-type monomer be hydrophobic, but rather that at least one of the positions in either the A- or B-type monomer must be hydrophobic to complete packing of the core.

**The Electrostatic Keystone Position**—The third residue in helix A2 is almost always positively charged (Lys), whereas the equivalent residue in helix B2 is almost always negatively charged (Asp or Glu) (Fig. 3). Examination of the structures revealed that these partially solvent-exposed keystone residues lie adjacent to the primarily hydrophobic interface between the two monomers as shown in Fig. 6A. Rather than interacting with each other, the keystone residues interact with complementary charged surfaces in the opposite monomer. The positively charged keystone residue in helix A2 packs against a negatively charged patch in helix B1 of the opposite monomer. Similarly, the negatively charged keystone residue in helix B2 lies adjacent to a positively charged patch in helix A1. These complementary electrostatic patches are present in all the L27 domain structures, although in each case, they are composed of varying residues whose identities are not absolutely conserved between L27 domains. Thus, in the context of A/B heterodimers, these keystone residues are found in a complementary electrostatic environment.

More important, if A/A or B/B homodimers were formed, these keystone residues would pack against a similarly charged patch (helix A2 with helix A1 and helix B2 with helix B1), resulting in a repulsive interaction. Thus, these keystone residues and their complementary electrostatic patch might make a significant contribution to preventing homodimer formation.

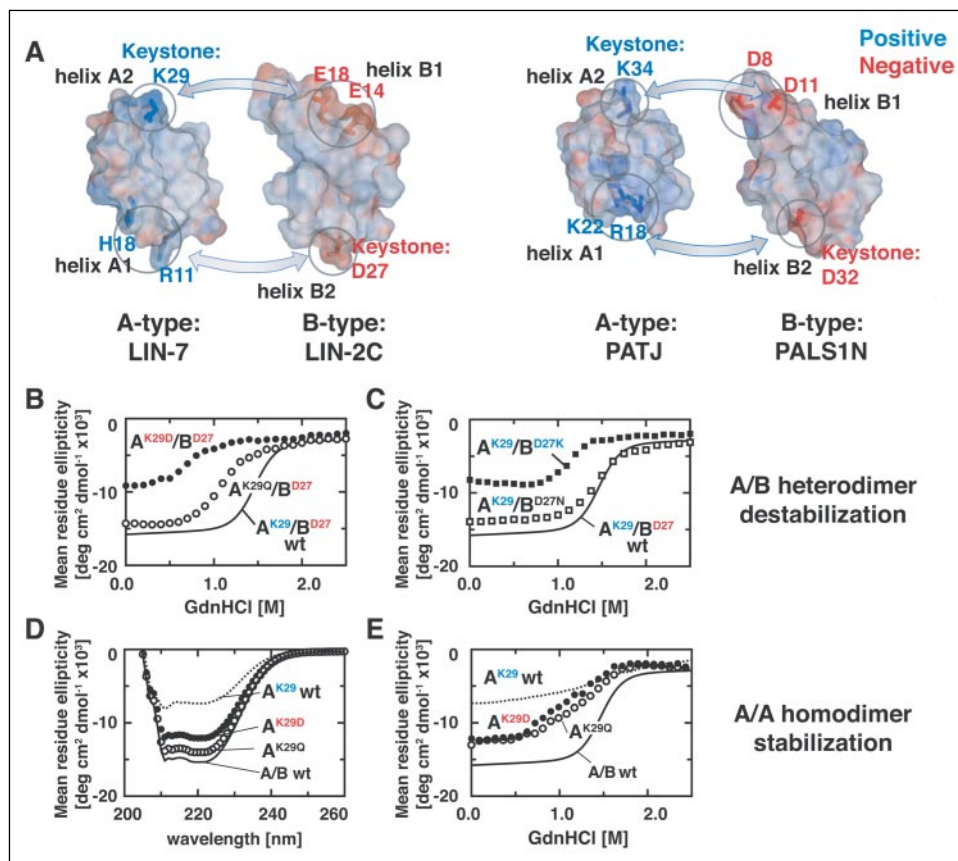
To examine the effect of these charged keystone residues on stabilization of the A/B heterodimer and destabilization of potential A/A and B/B homodimers, we mutated these residues in the context of the linked LIN-7/LIN-2C construct. The keystone residues were mutated to either an uncharged residue or a residue of opposite charge. If the charge interaction is critical for stabilizing the heterodimer, then mutation to either a neutral or oppositely charged residue will be highly destabilizing. If the primary role of the residue is to prevent potential homodimerization through charge repulsion, then one would expect to see dramatic destabilization only when these keystone residues are mutated to the opposite charge (*i.e.* if they are mutated to look more like a homodimeric partner), whereas a neutral residue would be tolerated.

The third residue in helix A2 of LIN-7 (residue 29 in the A-type monomer) is normally lysine. When Lys<sup>29</sup> was mutated to a neutral residue, glutamine (Fig. 6B), the protein displayed mild destabilization. However, more significant destabilization (reduced helicity and unfolding at lower denaturant concentrations) was observed when Lys<sup>29</sup> was mutated to aspartate (swapping its identity with that of the equivalent keystone residue in a B-type monomer). The K29D mutant showed behavior that began to approach that of an A/A homodimer pair: the CD signal under basal conditions was reduced, and the unfolding transition midpoint and sharpness were reduced.

The third residue in helix B2 of LIN-2 (residue 27 in the B-type monomer) is normally aspartate. When Asp<sup>27</sup> was mutated to a neutral residue, asparagine (Fig. 6C), the protein folding and stability were mildly reduced. A more significant destabilization was observed with mutation of Asp<sup>27</sup> to a positively charged residue, lysine, which made it mimic the keystone residue in an A-type monomer. The D27K mutant approached the B/B homodimer pair, showing effects similar to those observed with the K29D charge reversal mutation discussed above.

## A Model for Preferential L27 Domain Hetero-oligomerization

**FIGURE 6. Mutational analysis of the electrostatic keystone position.** *A*, surface electrostatic potentials are shown for the four-helix bundle of two L27 domain heterodimers. This is the top view, looking down the axis of the four-helix bundle; the monomers were pulled apart to view the interface. Electrostatic keystone residues in helices A2 and B2 (LIN-7 Lys<sup>29</sup> and LIN-2C Asp<sup>27</sup> or PATJ Lys<sup>34</sup> and PALS1N Asp<sup>32</sup>) interact with complementary charged surfaces on helices B1 and A1, respectively. In principle, homodimerization would lead to repulsive interactions. *B*, GdnHCl denaturation curves show that mutation of the positively charged keystone residue in the A-type monomer to a neutral residue (LIN-7 K29Q; ○) led to small decrease in stability; mutation to an oppositely charged residue (K29D; ●) led to more significant destabilization. *C*, mutation of the negatively charged keystone residue in the B-type monomer to a neutral residue (LIN-2C D27N; □) led to a small decrease in heterodimer stability; mutation to an oppositely charged residue (D27K; ■) led to more significant destabilization. *D*, the CD spectra show that LIN-7 alone has low helical content (---), whereas mutation of the positively charged keystone residue to an oppositely charge residue (K29D; ●) or a neutral residue (K29Q; ○) increased helical content close to that of the completely folded wild-type (wt) A/B heterodimer (—). *E*, LIN-7 alone does not show a cooperative GdnHCl unfolding transition (---). Mutation of the keystone residue to an oppositely charged residue (K29D; ●) or a neutral residue (K29Q; ○) yielded proteins showing significantly more cooperative unfolding transitions. The unfolding transition for the linked A/B heterodimer (—) is shown for reference. For all of these experiments, the total L27 domain concentration was 10 μM (10 μM monomers and 5 μM linked heterodimer). *deg*, degrees.



Together, these mutational results indicate that the electrostatic keystone residues make two contributions. The residues make a minor contribution to stabilizing the heterodimer, presumably through favorable electrostatic interactions. However, they make a more significant contribution to destabilizing potential homodimer formation via electrostatic repulsion.

As the residues composing the complementary electrostatic patch are not conserved between subclasses within the A- or B-types, these positions may be involved in further determining specificity within A and B subclasses. Mutations to neutral or opposite charge were destabilizing (data not shown). However, because these mutations may have destabilized the protein for reasons other than the complementary-keystone interactions, we addressed the importance of the electrostatic keystone position by designing a mutant predicted to stabilize homodimer formation.

**Artificial Stabilization of Homodimers**—These data support a model in which the electrostatic keystone residues play a key role in determining the relative stabilities of heterotypic *versus* homotypic dimers. A prediction of the model is that specific mutations of the keystone residues may allow for formation of stable homodimers. In our model, the homodimer association between two LIN-7 L27 domains is disfavored by repulsion between the positively charged residue (lysine) in the keystone position and the similarly positively charged surface on helix A1, surfaces that would come into contact in a putative homodimer (Fig. 6A).

Our model predicts that mutation of the keystone lysine to a negative or neutral residue should stabilize homodimer formation. To test this, we worked with a single A-type L27 domain (unlinked) from LIN-7 and mutated its electrostatic keystone residue (Lys<sup>29</sup>) to aspartic acid or glutamine. We observe several pieces of evidence indicating stabiliza-

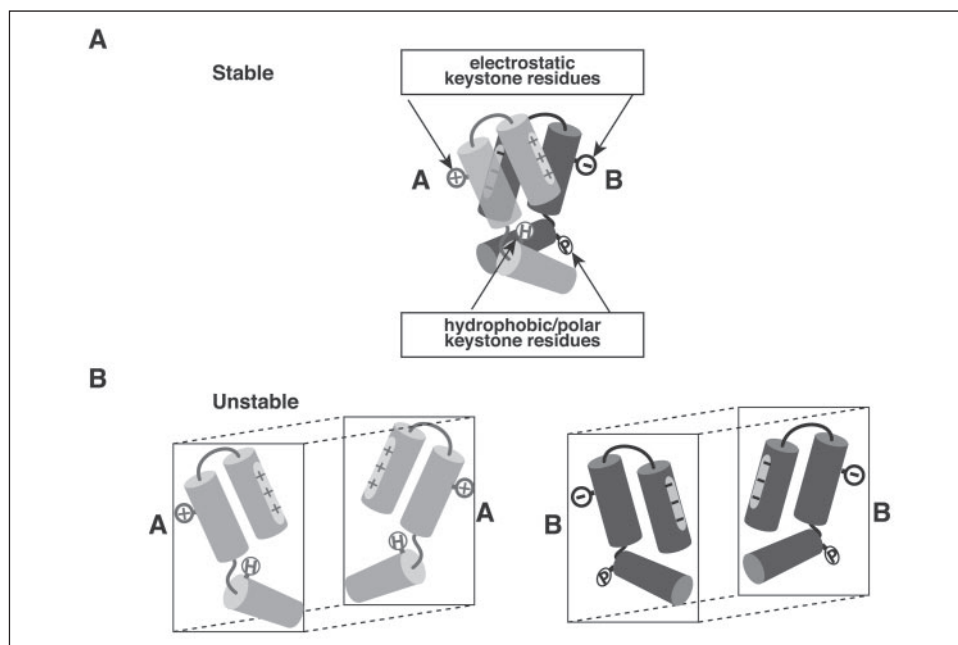
tion of a folded homomer structure (Fig. 6, *D* and *E*). First, the mutant LIN-7 L27 domains showed a dramatic increase in helical content by CD. Second, the mutant L27 domains showed a cooperative GdnHCl unfolding transition. Although this transition was not as sharp as with a native heterodimer pair, it was significantly more cooperative than the transition of the wild-type LIN-7 monomer. The observation that both the neutral substitution (K29Q) and the charge swap substitution (K29D) caused similar increases in stability suggests that removing the repulsive interaction is energetically more critical than potentially creating a stabilizing salt bridge (41).

## DISCUSSION

**A General Model for Preferential Heterotypic L27 Domain Assembly: Importance of Negative Design**—The analysis and experiments described here support a model of L27 domain assembly in which heterotypic dimer formation is favored, not simply because of high complementarity between heterotypic monomers, but also because of strong repulsion between homotypic monomers. As shown in Fig. 7, there are two keystone positions in each monomer that determine monomer type. One keystone residue, at the beginning of helix 2, is electrostatic: in A-type monomers, it is positively charged, whereas in B-type monomers, it is negatively charged. The second keystone residue, at the beginning of helix 3, can pack into the core at the base of the helical bundle: in A-type monomers, it is hydrophobic, whereas in B-type monomers, it is polar.

Two types of interactions determine whether a dimer complex will be stable. First, the electrostatic keystone residue must be complementary in charge to the surface on helix 2 of the partner monomer. A and B partners display the proper complementarity; however, A/A or B/B partners would be repulsive. As predicted, when charge swap mutations

**FIGURE 7. General model for how L27 domain keystone positions favor formation of heterotypic dimers, but disfavor homodimers.** The schematics show how two L27 domain monomers pack against one another to form a dimer. *A*, stable heterodimers have complementary electrostatic surfaces on helices 1 and 2 and have a hydrophobic residue at one of the keystone positions in helix 3, allowing for proper packing and closure of the hydrophobic core. (The charge on helix 1 is not conserved to one specific residue and is represented by a cloud indicating overall electrostatic potential.) *B*, we postulate that A/A and B/B homodimers are highly unstable because they would have repulsive interactions at the helix 1-helix 2 interface and cannot fulfill packing requirements.



are made at the electrostatic keystone residues in the context of the normally interacting A/B heterodimer, the interaction is severely destabilized because this interface mimics the repulsive interaction that would occur in a homodimer. Second, to properly cap the core of the central four-helix bundle, there appears to be a strong preference for a hydrophobic residue at one of the keystone residues at the beginning of helix 3. In the case of A/B heterodimers, it is the A-type monomer that always provides this large hydrophobic residue to complete packing of the core; the B-type monomer consistently has a polar residue at this position, leading to the conserved asymmetry in the A3 and B3 helix positions.

A critical element of this model is that L27 domain interaction specificity is determined not only by positive interactions made in the preferred A/B heterodimers, but also by strong negative interactions that would occur in the hypothetical A/A or B/B homodimers. We have been able to make specific loss-of-charge mutations that yielded a significantly stabilized A/A homodimer. Thus, L27 domains appear to have evolved through both positive and negative design to optimize obligate heterotypic interactions. Such tight interaction differences are compatible with the general function of L27 domains as modules that direct the assembly of large heteromeric supramolecular complexes.

The model presented here explains why the A and B types of L27 domains generally prefer heterotypic interactions; it does not explicitly explain why, within the class of A- and B-type monomers, specific domains preferentially interact with one another. Presumably, finer resolution interactions and differences between domains determine this higher level of specificity. Moreover, recent studies have suggested that domain-specific interactions formed in higher order tetrameric assemblies can play a role in specificity (31).

**Avoidance of Intramolecular Interaction in Proteins Containing Multiple L27 Domains**—Some proteins, including LIN-2 and its orthologs, are observed to have two adjacent L27 domains. In all of these known cases, the two domains are the B type (B/B). Each of these domains mediates interaction with a distinct protein containing an A-type monomer. For proper assembly of the complex to take place, it may be particularly important that the two L27 domains in the same protein do not interact with one another, especially given their high effective concentration. Having two adjacent domains of the same type and having

such a strongly disfavored homodimeric interaction, especially between B-type monomers, would prevent this potential competitive intramolecular association.

**Homo-oligomerization of SAP97 Family L27 Domains**—There is a small subset of L27 domains (three in human) that appear to lack at least one of the hallmark electrostatic keystone residues. The mammalian protein SAP97 and its invertebrate ortholog, DLG, align with A-type domains, but have a neutral residue at the normally positively charged keystone residue at the beginning of helix 2 (Fig. 3B). In our model, loss of this positively charged keystone residue would, in principle, increase the stability of the normally unfavorable L27 domain homodimer. Although the SAP97 L27 domain can form stable heterodimers with a B-type L27 domain from LIN-2 (29), recent studies have indicated that SAP97 and DLG proteins can also homo-oligomerize in an L27 domain-dependent manner (42, 43). This unique property among L27 domains is consistent with the rules for oligomerization presented here.

Heterotypic interactions of the SAP97 L27 domain are thought to be important for proper trafficking of synaptic receptors (44), and homodimeric interactions are thought to be important for proper functional assembly at synapses (42). Thus, the SAP97 family of L27 domains appears to have evolved to minimize homodimeric repulsion to allow the domains to participate in both homodimeric and heterodimeric interactions, a feature unique to this L27 domain family.

**Negative Design: Other Examples and Engineered Proteins**—L27 domains appear to use a remarkably simple repulsive mechanism to achieve high dimerization specificity. This type of negative design, the introduction of potential repulsive interactions that would selectively be made in an undesired complex, is observed in several other systems.

The importance of electrostatic repulsion in preventing L27 domain homodimerization is very similar to that of the mechanism of preferential heterodimerization observed in certain coiled coils. For example, the Fos leucine zipper does not form a stable homodimer, but instead forms a tight heterodimer with the Jun leucine zipper (45). This preference is largely driven by electrostatic repulsive interactions that would occur in a hypothetical Fos homodimer. In another example, artificial coiled coils can be designed to selectively homo- or hetero-dimerize according to negative selection against engineered interfaces with

## A Model for Preferential L27 Domain Hetero-oligomerization

repulsive charge interactions or unsatisfactory packing arrangements (46).

Introducing interactions that are repulsive or destabilizing in the context of only one of several possible interaction states has been used to greatly increase interaction specificity of engineered proteins (46, 47). Negative design, as illustrated by L27 domains, is a powerful force in optimizing protein-protein interaction specificity, whether achieved through evolution or design.

### REFERENCES

1. Park, S. H., Zarrinpar, A., and Lim, W. A. (2003) *Science* **299**, 1061–1064
2. Zarrinpar, A., Park, S. H., and Lim, W. A. (2003) *Nature* **426**, 676–680
3. Kennedy, M. B. (1997) *Trends Neurosci.* **20**, 264–268
4. Garner, C. C., Nash, J., and Haganir, R. L. (2000) *Trends Cell Biol.* **10**, 274–280
5. Mitic, L. L., and Anderson, J. M. (1998) *Annu. Rev. Physiol.* **60**, 121–142
6. Rudd, C. E. (1999) *Cell* **96**, 5–8
7. Harris, B. Z., and Lim, W. A. (2001) *J. Cell Sci.* **114**, 3219–3231
8. Dimitratos, S. D., Woods, D. F., Stathakis, D. G., and Bryant, P. J. (1999) *BioEssays* **21**, 912–921
9. Rongo, C. (2001) *Cytokine Growth Factor Rev.* **12**, 349–359
10. Kamberov, E., Makarova, O., Roh, M., Liu, A., Karnak, D., Straight, S., and Margolis, B. (2000) *J. Biol. Chem.* **275**, 11425–11431
11. Harris, B. Z., Venkatasubrahmanyam, S., and Lim, W. A. (2002) *J. Biol. Chem.* **277**, 34902–34908
12. Lee, S., Fan, S., Makarova, O., Straight, S., and Margolis, B. (2002) *Mol. Cell. Biol.* **22**, 1778–1791
13. Roh, M. H., Makarova, O., Liu, C. J., Shin, K., Lee, S., Laurinec, S., Goyal, M., Wiggins, R., and Margolis, B. (2002) *J. Cell Biol.* **157**, 161–172
14. Karnak, D., Lee, S., and Margolis, B. (2002) *J. Biol. Chem.* **277**, 46730–46735
15. Schultz, J., Milpetz, F., Bork, P., and Ponting, C. P. (1998) *Proc. Natl. Acad. Sci. U. S. A.* **95**, 5857–5864
16. Kaech, S. M., Whitfield, C. W., and Kim, S. K. (1998) *Cell* **94**, 761–771
17. Jo, K., Derin, R., Li, M., and Bredt, D. S. (1999) *J. Neurosci.* **19**, 4189–4199
18. Butz, S., Okamoto, M., and Sudhof, T. C. (1998) *Cell* **94**, 773–782
19. Borg, J. P., Straight, S. W., Kaech, S. M., de Taddeo-Borg, M., Kroon, D. E., Karnak, D., Turner, R. S., Kim, S. K., and Margolis, B. (1998) *J. Biol. Chem.* **273**, 31633–31636
20. Thomas, U., Kim, E., Kuhlendahl, S., Koh, Y. H., Gundelfinger, E. D., Sheng, M., Garner, C. C., and Budnik, V. (1997) *Neuron* **19**, 787–799
21. Bachmann, A., Timmer, M., Sierralta, J., Pietrini, G., Gundelfinger, E. D., Knust, E., and Thomas, U. (2004) *J. Cell Sci.* **117**, 1899–1909
22. Hong, Y., Stronach, B., Perrimon, N., Jan, L. Y., and Jan, Y. N. (2001) *Nature* **414**, 634–638
23. Bachmann, A., Schneider, M., Theilenberg, E., Grawe, F., and Knust, E. (2001) *Nature* **414**, 638–643
24. Shin, K., Straight, S., and Margolis, B. (2005) *J. Cell Biol.* **168**, 705–711
25. Straight, S. W., Shin, K., Fogg, V. C., Fan, S., Liu, C. J., Roh, M., and Margolis, B. (2004) *Mol. Biol. Cell* **15**, 1981–1990
26. Ralston, K. J., Hird, S. L., Zhang, X., Scott, J. L., Jin, B., Thorne, R. F., Berndt, M. C., Boyd, A. W., and Burns, G. F. (2004) *J. Biol. Chem.* **279**, 33816–33828
27. Round, J. L., Tomassian, T., Zhang, M., Patel, V., Schoenberger, S. P., and Miceli, M. C. (2005) *J. Exp. Med.* **201**, 419–430
28. Doerks, T., Bork, P., Kamberov, E., Makarova, O., Muecke, S., and Margolis, B. (2000) *Trends Biochem. Sci.* **25**, 317–318
29. Feng, W., Long, J. F., Fan, J. S., Suetake, T., and Zhang, M. (2004) *Nat. Struct. Mol. Biol.* **11**, 475–480
30. Li, Y., Karnak, D., Demeler, B., Margolis, B., and Lavie, A. (2004) *EMBO J.* **23**, 2723–2733
31. Feng, W., Long, J. F., and Zhang, M. (2005) *Proc. Natl. Acad. Sci. U. S. A.* **102**, 6861–6866
32. Salzmann, M. W. G., Pervushin, K., Senn, H., and Wuthrich, K. (1999) *J. Am. Chem. Soc.* **121**, 844–848
33. Deleted in proof
34. Bartels, C., Xia, T., Billeter, M., Güntert, P., and Wüthrich, K. (1995) *J. Biomol. NMR* **6**, 1–10
35. Cornilescu, G., Delaglio, F., and Bax, A. (1999) *J. Biomol. NMR* **13**, 289–302
36. Güntert, P., Mumenthaler, C., and Wüthrich, K. (1997) *J. Mol. Biol.* **273**, 283–298
37. Brünger, A. T., Adams, P. D., Clore, G. M., DeLano, W. L., Gros, P., Grosse-Kunstleve, R. W., Jiang, J. S., Kuszewski, J., Nilges, M., Pannu, N. S., Read, R. J., Rice, L. M., Simonson, T., and Warren, G. L. (1998) *Acta Crystallogr. Sect. D Biol. Crystallogr.* **54**, 905–921
38. Laskowski, R. A., Rullmann, J. A., MacArthur, M. W., Kaptein, R., and Thornton, J. M. (1996) *J. Biomol. NMR* **8**, 477–486
39. Koradi, R., Billeter, M., and Wüthrich, K. (1996) *J. Mol. Graph.* **14**, 51–55
40. DeLano, W. L. (2002) The PyMOL Molecular Graphics System, DeLano Scientific, San Carlos, CA
41. Sheinerman, F. B., Norel, R., and Honig, B. (2000) *Curr. Opin. Struct. Biol.* **10**, 153–159
42. Nakagawa, T., Futai, K., Lashuel, H. A., Lo, I., Okamoto, K., Walz, T., Hayashi, Y., and Sheng, M. (2004) *Neuron* **44**, 453–467
43. Marfatia, S. M., Byron, O., Campbell, G., Liu, S. C., and Chishti, A. H. (2000) *J. Biol. Chem.* **275**, 13759–13770
44. Leonoudakis, D., Conti, L. R., Radeke, C. M., McGuire, L. M., and Vandenberg, C. A. (2004) *J. Biol. Chem.* **279**, 19051–19063
45. O’Shea, E. K., Rutkowski, R., and Kim, P. S. (1992) *Cell* **68**, 699–708
46. Havranek, J. J., and Harbury, P. B. (2003) *Nat. Struct. Mol. Biol.* **10**, 45–52
47. Kortemme, T., Joachimiak, L. A., Bullock, A. N., Schuler, A. D., Stoddard, B. L., and Baker, D. (2004) *Nat. Struct. Mol. Biol.* **11**, 371–379